Abhay B. Ramachandra
Department of Biomedical Engineering,
Yale University,
New Haven, CT 06520
e-mail: abhay.ramachandra@yale.edu

Nicole Mikush
Translational Research Imaging Center,
Yale School of Medicine,
New Haven, CT 06520
e-mail: nicole.mikush@yale.edu

Maor Sauler
Section of Pulmonary, Critical Care, and
Sleep Medicine,
Department of Internal Medicine,
Yale School of Medicine,
New Haven, CT 06510
e-mail: maor.sauler@yale.edu

Jay D. Humphrey
Department of Biomedical Engineering and
Vascular Biology and Therapeutics Program,
Yale University,
New Haven, CT 06520
e-mail: jay.humphrey@yale.edu

Edward P. Manning[1]
Section of Pulmonary, Critical Care, and
Sleep Medicine,
Department of Internal Medicine,
Yale School of Medicine,
New Haven, CT 06510;
West Haven Connecticut VA and Pulmonary and
Critical Care Medicine,
VA Connecticut Healthcare System,
West Haven, CT 06516
e-mail: edward.manning@yale.edu

Compromised Cardiopulmonary Function in Fibulin-5 Deficient Mice

Competent elastic fibers are critical to the function of the lung and right circulation. Murine models of elastopathies can aid in understanding the functional roles of the elastin and elastin-associated glycoproteins that constitute elastic fibers. Here, we quantify together lung and pulmonary arterial structure, function, and mechanics with right heart function in a mouse model deficient in the elastin-associated glycoprotein fibulin-5. Differences emerged as a function of genotype, sex, and arterial region. Specifically, functional studies revealed increased lung compliance in fibulin-5 deficiency consistent with a histologically observed increased alveolar disruption. Biaxial mechanical tests revealed that the primary branch pulmonary arteries exhibit decreased elastic energy storage capacity and wall stress despite only modest differences in circumferential and axial material stiffness in the fibulin-5 deficient mice. Histological quantifications confirm a lower elastic fiber content in the fibulin-5 deficient pulmonary arteries, with fragmented elastic laminae in the outer part of the wall - likely the reason for reduced energy storage. Ultrasound measurements confirm sex differences in compromised right ventricular function in the fibulin-5 deficient mice. These results reveal compromised right heart function, but opposite effects of elastic fiber dysfunction on the lung parenchyma (significantly increased compliance) and pulmonary arteries (trend toward decreased distensibility), and call for further probing of ventilation-perfusion relationships in pulmonary pathologies. Amongst many other models, fibulin-5 deficient mice can contribute to our understanding of the complex roles of elastin in pulmonary health and disease.
[DOI: 10.1115/1.4053873]

Keywords: elastin, fibulin, emphysema, ventilation-perfusion, sex difference, biomechanical phenotyping

Introduction

The lung comprises two parallel transport networks embedded within the parenchyma, one for ventilation and one for blood perfusion, which work concomitantly to promote organ function [1]. Connective tissue defects, both congenital and acquired, can alter the balance in these two coupled networks and drive the pulmonary system toward maladaptation, with potential feedback that affects right heart function [2–4]. The multifactorial mechanisms of cardiopulmonary mechanics and physiology in humans have made it challenging to understand pathologic maladaptations, including cases of congenital connective tissue disorders as well as acquired conditions such as chronic obstructive pulmonary disease (COPD) and pulmonary arterial hypertension [5–8]. Mouse models provide an opportunity to study some of these mechanisms in isolation [9,10].

Here we probe the microstructure and mechanical function of the lung and primary branch pulmonary arteries in a mouse model of compromised elastic-fiber integrity generated via a germline mutation of the gene (*Fbln5*) that encodes the elastin-associated glycoprotein fibulin-5 [11,12], which plays critical roles in elastogenesis. Cross-linked elastin, the core structural protein of elastic fibers, is central to elastic recoil of both the lungs and pulmonary arteries, the latter when distended under systolic pressures. Compromised elastic fibers can lead to multiple pulmonary pathologies, including emphysema, a pathologic manifestation of COPD [2,13]. Elastin insufficiency has also been associated with pulmonary arterial hypertension [14]. Amongst the consequences of fibulin-5 deficiency in mice are severe emphysema, right ventricle enlargement, and right heart failure [11]. Fibulin-5 null mice exhibit disrupted distal airways as early as postnatal day 3 (P3) and enlargement of distal airspaces by P14 [11,12]. While prior work has reported such changes using structural metrics, detailed quantification of pulmonary function, pulmonary arterial mechanics, and right heart function have remained wanting.

Most studies of pulmonary pathologies have probed roles of the lung parenchyma, airways, and pulmonary vasculature in isolation, with few quantifying pulmonary function, vascular properties, and cardiac function [15]. The current study addresses this gap in knowledge at the tissue level. Changes in the mechanical behaviors of the lung parenchyma and pulmonary arteries can alter the ventilation-perfusion relationship within the cardiopulmonary system [16]. Thus, coordinated characterizations of the lung, vascular, and cardiac structure and function represent an essential step toward uncovering biomechanical mechanisms that couple ventilation and hemodynamics within the pulmonary system at the tissue level. Here, we use whole lung inflation tests to quantify lung function, biaxial mechanical testing to quantify

[1]Corresponding author.
Manuscript received September 22, 2021; final manuscript received February 8, 2022; published online March 11, 2022. Assoc. Editor: Craig Goergen.

passive pulmonary artery mechanics, and transthoracic echocardiography to quantify right heart function in adult male and female mice that are either wild-type (WT) or deficient (KO) in fibulin-5. The vascular biaxial protocols were derived from our previous work on C57BL/6J WT mice [17], which in turn emerged from our previous systemic artery protocols (e.g., Refs. [18–20]). We have used echocardiography to quantify left cardiac function (e.g., [21–23]), but this is the first time we quantify both right heart function using echo and lung function using pulmonary function tests (PFT), with associated histological measurements in the same mouse model. Quantification of vascular, right heart, and lung structure and function provide a more complete picture at the system level in an elastic fiber compromised mouse. Motivated by prior studies on regional differences in pulmonary pathologies [24–26], we also compare potential differences in the mechanics of the right and left pulmonary artery. Finally, we compare histological differences in the pulmonary parenchyma, vasculature, and the right ventricle due to changes in elastic fibers.

Methods

Animal Studies. All live animal protocols were approved by the Institutional Animal Care and Use Committee of Yale University. Homozygous *Fbln5*$^{+/+}$ (WT) and *Fbln5*$^{-/-}$ (KO) adult mice, on a mixed C57BL/6 x 129/SvEv background, were divided into four groups: female WT (FWT), male WT (MWT), female KO (FKO), and male KO (MKO).

Pulmonary Function Tests: Adult mice (20-30 weeks old; FWT: n = 5, MWT: n = 6, FKO: n = 5, MKO: n = 6) were anesthetized using urethane (1 g/kg administered in 10% solution with sterile water), tracheostomized, and then connected to a FlexiVent® system (SCIREQ©, Montreal, QC, Canada). Succinylcholine (1 mg/kg) was administered via intraperitoneal injection to eliminate spontaneous breathing. FlexiVent perturbations and oscillations were analyzed using FlexiWare software (version 7.6, Service Pack 6) to obtain lung pressure–volume loops and static compliance (*Cst*). Maneuvers and perturbations were continued until acquiring three suitable measurements. A coefficient of determination of 0.95 defined the lower limit for suitable measurements. An average of three measurements for each parameter was calculated per mouse. More details on the methods can be found in our previous work [27,28].

Echocardiography: Noninvasive investigation of cardiac function was performed in additional adult mice from all four groups (FWT: n = 5, MWT: n = 4, FKO: n = 4, MKO: n = 3) using transthoracic echocardiograms under light anesthesia (1.5% isoflurane) while maintaining physiological temperatures [29]. Standardized cardiac views were obtained with a high-resolution ultrasound system (Vevo 2100, VisualSonics, Toronto, ON, Canada) equipped with an ultrahigh frequency (40 MHz) linear array transducer. Right ventricle outflow tract (RVOT) diameter, tricuspid annular plane systolic excursion (TAPSE), pulmonary artery acceleration time (PAT), pulmonary ejection time (PET), two-dimensional end systolic (ES) and diastolic (ED) right ventricle area, and right atrial (RA) area were measured offline using Vevo Lab software (version 3.2.6, VisualSonics) by an experienced sonographer. Fractional area change of the right ventricle was computed as (ED-ES)/ED × 100 [30].

Arterial Biomechanical Testing: Additional adult mice (18–22 weeks old; Right Pulmonary Artery (RPA) - n = 6 per group and Left Pulmonary Artery (LPA) - FWT: n = 5, MWT: n = 7, FKO: n = 6, MKO: n = 6) were euthanized with an intraperitoneal injection of Beuthanasia-D and branch pulmonary arteries were excised for biaxial testing. Specifically, RPA and LPA were dissected from the main pulmonary artery to the first bifurcation of the branch pulmonary arteries and prepared for biaxial testing as described previously [17]. Briefly, perivascular tissue and fat were gently removed and the branches were ligated with suture. The vessels were mounted on custom glass pipettes and secured with a 6-0 suture, with proximal sections secured at the bifurcation from the main pulmonary artery and distal sections secured at the first branching of the branch pulmonary artery. Vessels were mounted in a bath containing Hanks buffered saline solution (HBSS) at room temperature for passive biaxial testing. The vessels were equilibrated for 15 min at a pressure of ~15 mmHg and subject-specific values of the in vivo axial stretch, then preconditioned with six cycles of pressurization from 5 to 40 mmHg; all data reported are following preconditioning. The testing protocol consisted of seven tests: pressure-distension tests at three different fixed values of axial stretch (subject-specific in vivo as well as 5% below and 5% above this value) and axial force-extension tests at four different fixed values of pressure (5, 15, 25 and 40 mmHg, with the highest value selected given possible elevations to these levels in pulmonary artery hypertension). Outer diameter was tracked with a video microscope and custom software; length was controlled with a submicron resolution stepper motor; axial force and pressure were measured with standard transducers.

Vascular constitutive modeling: Passive mechanics of the pulmonary arteries was modeled using a 2-D formulation since residual stresses tend to homogenize the transmural distribution of wall stress [31], thus allowing radially averaged (mean) values to represent the stresses well. Mean values of the Cauchy wall stresses in circumferential (θ) and axial (z) directions are given by

$$\sigma_\theta = \frac{Pr_i}{r_o - r_i} \quad \text{and} \quad \sigma_z = \frac{f_T + P\pi r_i^2}{\pi(r_o^2 - r_i^2)}$$

where P is the transmural pressure, r_i is the deformed inner radius, r_o is the deformed outer radius, and f_T is the transducer measured axial force. Under the assumption of incompressibility, inner radius $r_i = \sqrt{r_o^2 - \bar{V}/\pi l}$, where l is the instantaneous length between the ligatures securing the vessel to the cannulae, and $\bar{V}$ is the volume of the vessel in the unloaded state. $\bar{V} = \frac{\pi}{4}(OD^2 - ID^2)L$ where L is the unloaded length, OD is the unloaded outer diameter, and $ID = OD - 2H$ is the unloaded inner diameter; note, H is the unloaded wall thickness.

A pseudo-elastic constitutive formulation, which has successfully described passive biaxial behaviors of pulmonary arteries [17], was used to quantify the passive mechanical behavior in terms of the stored energy function, W. The stress and material stiffness are computed via first and second derivatives of W with respect to an appropriate measure of the deformation. Based on success of prior work, let

$$W = \frac{c}{2}(I_c - 3) + \sum_{i=1}^{4} \frac{c_1^i}{4c_2^i}\left\{\exp\left[c_2^i\left(IV_c^i - 1\right)^2\right] - 1\right\}$$

where c, c_1^i and c_2^i are material parameters; $i = 1, 2, 3, 4$ denote four fiber families along axial, circumferential, and two symmetric diagonal (measured by angle α_0 with respect to the axial direction) directions, respectively. $I_c = \lambda_\theta^2 + \lambda_z^2 + 1/\lambda_z^2\lambda_\theta^2$ is the first invariant of right Cauchy-Green tensor $\mathbf{C}$ and $IV_c^i = \lambda_\theta^2 \sin^2\alpha_0^i + \lambda_z^2 \cos^2\alpha_0^i$ is the square of the stretch of the i^{th} fiber family, also computed in terms of $\mathbf{C}$; $\lambda_\theta = (r_i + r_o)/2\rho_{\text{mid}}$ and $\lambda_z = l/L$ are the mean circumferential and axial stretches, with ρ_{mid} the unloaded midwall radius, and α_0^i is the fiber angle relative to axial direction in the reference configuration. Best-fit values of the constitutive model parameters (c, c_1^1 and c_2^1, c_1^2, c_2^2, $c_1^{3,4}$, $c_2^{3,4}$ and α_0^i) were obtained by minimizing the following objective function (using *lsqnonlin* in MATLAB with a *trust-region-reflective* option, tolerance = 1×10^{-10})

$$J = \sum_{i=1}^{N}\left[\left(\frac{P^{th} - P^{\exp}}{\bar{P}^{\exp}}\right)_i^2 + \left(\frac{f^{th} - f^{\exp}}{\bar{f}^{\exp}}\right)_i^2\right]$$

where N is the number of equilibrium states (hundreds when combining data from seven protocols), *th* denotes theoretically computed, *exp* denotes experimentally measured, and an overbar denotes a mean value. Bounds for the parameters

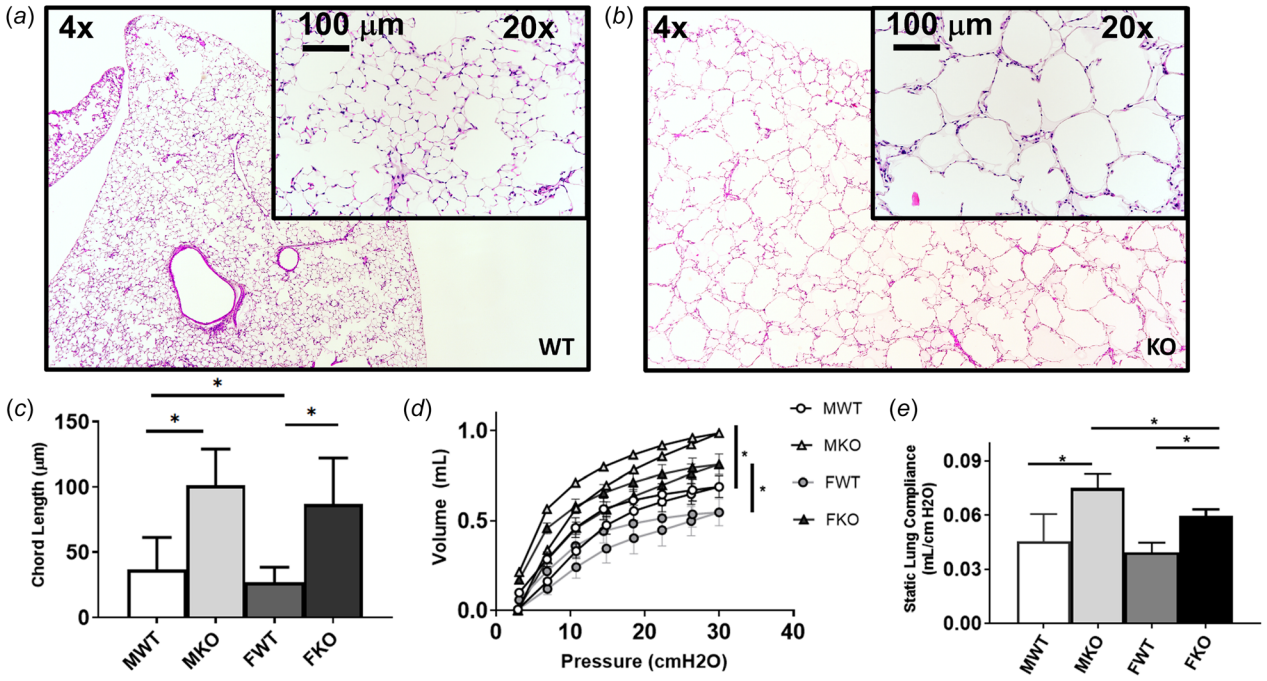

Fig. 1 Representative hematoxylin and eosin (H&E) stained sections of lungs from *Fbln5*$^{+/+}$ (WT; (*a*)) and *Fbln5*$^{-/-}$ (KO, (*b*)) mice shown at 4X and 20X magnification (inset). Chord Length analysis of the H&E sections ((*c*); mean±SEM; FWT: n = 5, FKO: n = 5, MWT: n = 5, MKO: n = 5). Pressure-volume relationships ((*d*); mean ± SEM) and associated static compliance ((*e*); mean ± SEM; FWT: n = 5, FKO: n = 5, MWT: n = 6, MKO: n = 6) from pulmonary function tests. female (F), male (M). * $p < 0.05$.

$[c, c_1^1, c_2^1, c_1^2, c_2^2, c_1^{3,4}, c_2^{3,4}, \alpha_0^i]$ were $[0, 0, 1 \times 10^{-6}, 0, 1 \times 10^{-6}, 0, 1 \times 10^{-6}, 0]$ and $[1 \times 10^5, 1 \times 10^5, 1 \times 10^5, 1 \times 10^5, 1 \times 10^5, 1 \times 10^5, 1 \times 10^5, \pi/2]$, similar to those used previously [18,32]. Converged values of the parameters were assessed using three random sets of initial guesses. More details on parameter estimation can be found in our prior work [17–19,32].

Histology: Immediately following the pulmonary functional analysis, the lungs were removed from the mouse with tracheal cannulation intact and inflated with warm (37 °C), 1% (weight:volume) low melting weight agarose in Phosphate-buffered Saline (PBS) × 1 at a pressure of 20 cmH_2O. The agarose solution was allowed to cool, the tracheal cannula was removed, the trachea was ligated, and the stiffened agarose-lung preparation was placed in 10% formalin for 24 h, then transferred to 70% ethanol. Similarly, unpressurized hearts were placed in 10% formalin and then transferred to 70% ethanol. Preparations were embedded in paraffin, sectioned with a microtome, then stained with hematoxylin and eosin (H&E) for imaging and analysis. Two slides from each mouse lung were analyzed and electronically imaged at 20× magnification (n = 5 per group). The chord length ImageJ plug-in was used to quantify lung morphometry in 20× magnification images of samples from each mouse [33]. At least ten samples of 20× magnification images for each slide were analyzed while focusing on lung parenchyma to avoid larger airways or vessels (n = 5 per group). Hearts were imaged at 4× magnification and two sections per sample (n = 4 per group) were analyzed for right ventricle (RV) thickness and area using ImageJ.

After biaxially testing the RPA and LPA, these vessels were fixed in neutral buffered 10% formalin while unloaded, then stored in 70% ethanol at 4 °C for histology. LPA samples were embedded in paraffin, sectioned, stained with Verhoeff's Van Gieson (VVG) or Masson's Trichrome (MTC), and imaged with an Olympus BX/51 microscope and Olympus DP70 digital camera (n = 3 per group). Complete cross section were considered by stitching subimages using Microsoft Image Composite Editor software. Wall constituents were quantified using custom software [19,32]. Briefly, following background subtraction and pixel thresholding, area fractions were computed as the ratio of pixels corresponding to a constituent divided by the total number of pixels in the image. Elastic fiber area fraction was quantified using VVG while cytoplasm fraction was quantified using MTC. Assuming GAG content was negligible at this age [19,21], collagen area fraction was computed as 1 - area fractions of elastin and cytoplasm [17,21]. We report histology results for the left pulmonary arteries.

Statistics: Normality of a variable in a group was probed using a Shapiro-Wilk test ($p < 0.05$ considered not normal). For variables distributed normally, a one-way ANOVA with Tukey's post-hoc analysis was used to probe potential statistical differences in morphological and mechanical properties between the groups. For variables not distributed normally, a nonparametric test (Kruskal Wallis) was used to assess possible differences. Results are presented as mean±standard error of the mean (SEM), where appropriate. A p value less than 0.05 was the threshold for statistical significance.

Results

In comparison to agarose-inflated lungs from female and male WT mice, those from female and male KO mice exhibited notable emphysematous-changes upon histological examination (Figs. 1(*a*) and 1(*b*), Figure S1 available in the Supplemental Materials on the ASME Digital Collection), with the mean alveolar chord length for KO (FKO: 86.98 ± 4.07 μm, MKO: 101.4 ± 3.76 μm) significantly greater than for WT (FWT: 26.71 ± 1.29 μm, MWT 36.42 ± 3.11 μm; Fig. 1(*c*)). Consistent with these observed structural changes in the parenchyma, pulmonary function testing revealed significantly higher lung volumes during mechanical ventilation (e.g., at a peak pressure of 30 cmH_2O, Fig. 1(*d*)), and thus higher mean lung compliance in KO (FKO: 0.060 ± 0.004 ml/cmH_2O, MKO: 0.075 ± 0.002 ml/cmH_2O), compared to WT (FWT:0.039 ± 0.006 ml/cmH_2O, MWT: 0.045 ± 0.004 ml/cmH_2O), in both sexes (Fig. 1(*e*)). The static lung compliance was also significantly different between

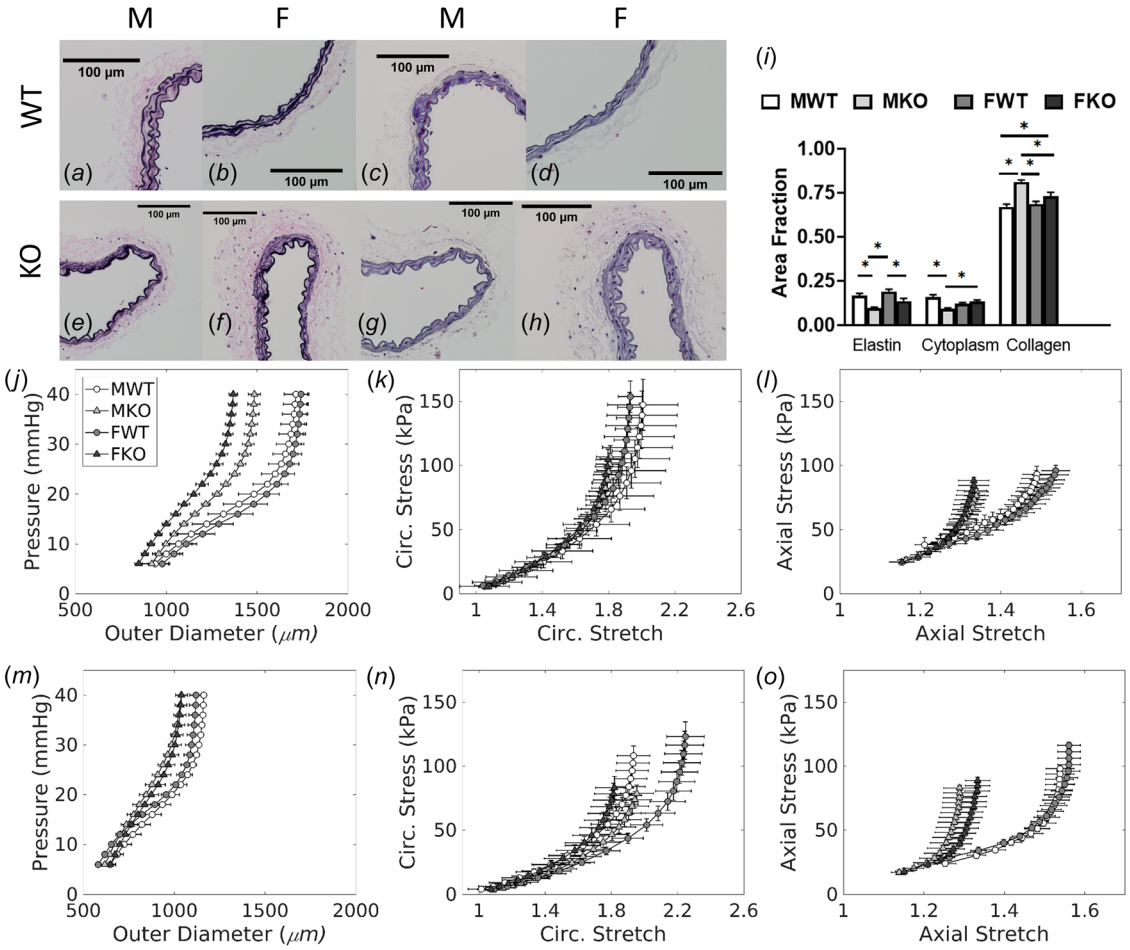

Fig. 2 Representative Verhoeff-Van Gieson (*a*, *b*, *e*, *f*) and Masson's Trichrome (*c*, *d*, *g*, *h*) stained cross sections for the left pulmonary arteries (LPAs) from *Fbln5*$^{+/+}$ (WT—top row) and *Fbln5*$^{-/-}$ (KO-bottom row) mice. Area fraction quantifications (i; mean ± SEM) are based on n ∼ 15 sections per stain per group with 3 biological replicates per group. Passive mechanical behavior of the right (RPA—middle row) and left (LPA—bottom row) pulmonary arteries from female (F) and male (M) *Fbln5*$^{+/+}$ (WT) and *Fbln5*$^{-/-}$ (KO) mice: pressure-diameter (j, m), and associated circumferential (k and n) and axial (l and o) Cauchy stress–stretch behaviors, averaged at vessel-specific in vivo stretches (mean ± SEM). RPA (FWT: n = 6, FKO: n = 6, MWT: n = 6, MKO: n = 6) and LPA (FWT: n = 5, FKO: n = 6, MWT: n = 7, MKO: n = 6).

female and male KOs. Note that the emphysematous changes seen in KO mice may have appeared greater in measurements of pulmonary structure obtained on *ex vivo* lungs as chest resistance is absent.

Representative VVG and MTC stained histological cross sections are shown in Fig. 2 for representative pulmonary arteries from all four groups. As expected, WT pulmonary arteries show organized, wavy, elastin laminae on VVG staining (Figs. 2(*a*) and 2(*b*)). While the KO arteries preserve this general structure, only the internal elastic lamina appeared intact (Figs. 2(*e*) and 2(*f*)); outer laminae were fragmented. Elastin area fraction was thus reduced in the KO vessels (FKO: 0.137 ± 0.015, MKO: 0.096 ± 0.007) relative to WT (FWT:0.191 ± 0.011, MWT:0.169 ± 0.011), which was significant in both females and males (Fig. 2(*i*)). Cytoplasm area fraction was significantly different between male WT and KO (MWT: 0.161 ± 0.012, MKO: 0.092 ± 0.007; Fig. 2(*i*)), but not females (FWT: 0.122 ± 0.007, FKO: 0.133 ± 0.009). Significant sex differences were observed in cytoplasm area fractions between female and male KO groups (FKO: 0.133 ± 0.009, MKO: 0.092 ± 0.007; Fig. 2(*i*)), however. Notwithstanding inter-relations among collagen, cytoplasm, and elastin area fractions, differences in collagen area fraction were significant between male WT and KO (MWT: 0.670 ± 0.015, MKO: 0.812 ± 0.011) and female KO and male KO groups (FKO: 0.73 ± 0.023, MKO: 0.812 ± 0.011; Fig. 2(*i*)); see also Fig. S2 available in the Supplemental Materials on the ASME Digital Collection. Mean structural and biaxial material behaviors are summarized in Fig. 2 for the right (RPA) and left (LPA) pulmonary artery from WT and KO mice, female and male. The pressure-diameter curves show averaged responses at specimen-specific fixed in vivo axial stretches (Figs. 2(*j*) and 2(*m*)). The KO vessels were generally less distensible than the WT vessels in both sexes and regions, namely, RPA and LPA (Figs. 2(*j*) and 2(*m*)). The circumferential and axial stress–stretch behaviors for the KO groups similarly suggested a stiffer material behavior (Figs. 2(*k*), 2(*l*), 2(*n*), and 2(*o*)), though this is best inferred from direct calculations (see below and Fig. 3). Nonetheless, the leftward shift in the KO stress–stretch curves was more pronounced along the axial direction (Figs. 2(*l*) and 2(*o*)).

Best-fit values of the eight constitutive model parameters are summarized in Table S1 available in the Supplemental Materials on the ASME Digital Collection for the RPA and LPA. Multiple passive mechanical metrics of interest were then computed at a representative pulmonary arterial pressure of 25 mmHg and specimen-specific in vivo stretch (Fig. 3). Significant differences in unloaded diameter were only found between FWT and MWT in LPAs (FWT: 564.00 ± 18.14 μm, MWT: 661.70 ± 27.98 μm; Fig. 3(*a*)). Loaded outer diameter was significantly lower in

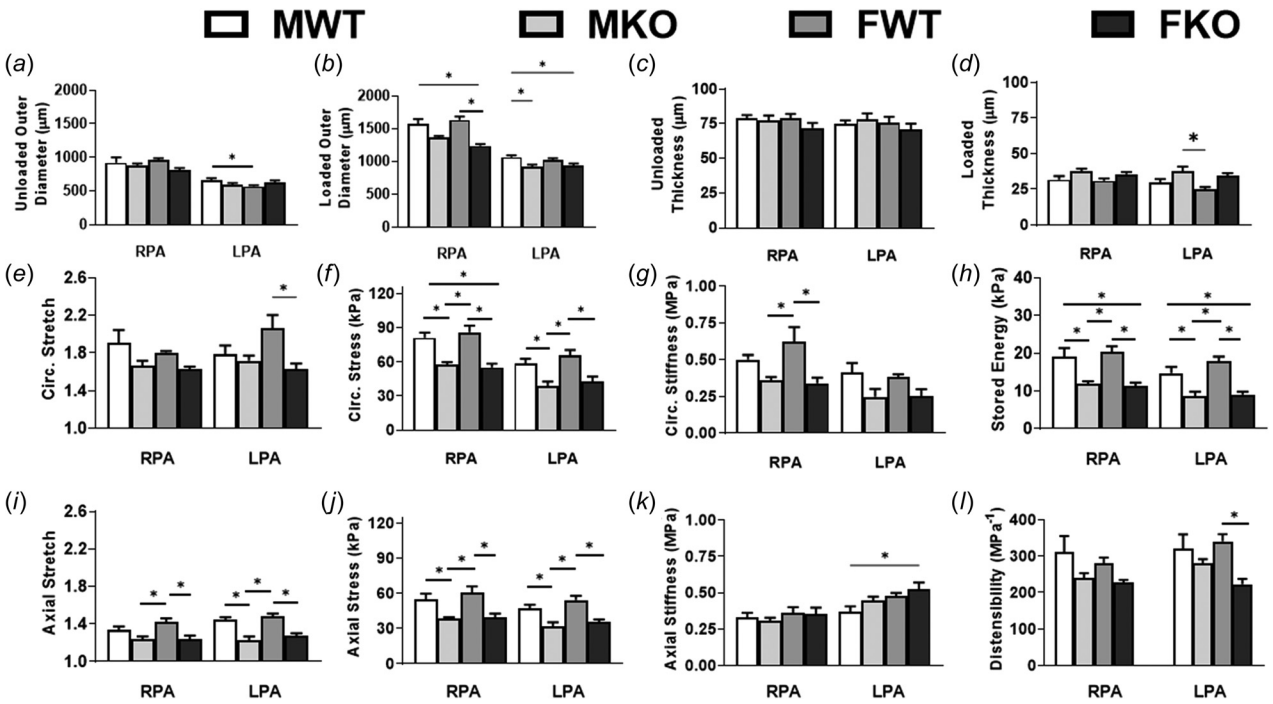

Fig. 3 Comparison of mechanical and morphometric metrics (mean±SEM) for the primary pulmonary arteries compared across genotypes, regions, and sex for *Fbln5*$^{+/+}$(WT) and *Fbln5*$^{-/-}$ (KO) mice; all loaded values are calculated at 25 mmHg and subject-specific in vivo axial stretch. Female (F), male (M); RPA (FWT: n = 6, FKO: n = 6, MWT: n = 6, MKO: n = 6) and LPA (FWT: n = 5, FKO: n = 6, MWT: n = 7, MKO: n = 6). *$p < 0.05$.

RPAs of female KOs and LPAs of male KOs compared to the corresponding WTs (RPA: FWT: 1631.00 ± 54.64 μm, FKO: 1240.00 ± 26.11 μm; LPA: MWT: 1067 ± 25.98 μm, MKO:919.7 ± 30.62 μm; Fig. 3(*b*)). No significant differences were observed in unloaded (Fig. 3(*c*)) or loaded (Fig. 3(*d*)) thickness between genotypes (WT versus KO) or sexes (F versus M). Circumferential stretch was significantly lower in female KO LPAs alone compared to WTs (FWT: 2.07 ± 0.14, FKO: 1.63 ± 0.06; Fig. 3(*e*)) while circumferential stress was significantly lower in KOs (RPA: FWT: 85.96 ± 6.00 kPa, FKO: 55.28 ± 3.29 kPa, MWT: 81.18 ± 4.47 kPa, MKO: 57.49 ± 2.48 kPa; LPA: FWT: 65.79 ± 4.57 kPa, FKO: 43.10 ± 4.13 kPa, MWT: 58.67 ± 4.33 kPa, MKO: 39.08 ± 3.79 kPa; Fig. 3(*f*)). Circumferential stiffness was significantly lower only in the female KO RPAs (RPA: FWT: 0.62 ± 0.10 MPa, FKO: 0.34 ± 0.04 MPa; Fig. 3(*g*)) while elastically stored energy was significantly lower in both female and male KOs compared to the corresponding WTs (RPA: FWT: 20.31 ± 1.51 kPa, FKO: 11.45 ± 0.83 kPa, MWT: 19.21 ± 2.15 kPa, MKO: 11.96 ± 0.65 kPa; LPA: FWT: 17.95 ± 1.20 kPa, FKO: 9.07 ± 0.75 kPa, MWT: 14.79 ± 1.61 kPa, MKO: 8.76 ± 1.09 kPa; Fig. 3(*h*)). Axial stretch was significantly lower in KOs, except in male RPAs (RPA: FWT: 1.42 ± 0.04, FKO: 1.24 ± 0.04, LPA: FWT: 1.48 ± 0.03, FKO: 1.28 ± 0.03, MWT: 1.44 ± 0.03, MKO: 1.23 ± 0.04; Fig. 3(*i*)). Axial stress was significantly lower in KOs compared to WTs (RPA: FWT: 60.79 ± 5.22 kPa, FKO: 39.35 ± 3.43 kPa, MWT: 54.65 ± 5.06 kPa, MKO: 38.48 ± 1.20 kPa; LPA: FWT: 54.18 ± 3.67 kPa, FKO: 35.67 ± 2.04 kPa, MWT:46.98 ± 3.40 kPa, MKO: 31.73 ± 3.54 kPa; Fig. 3(*j*)) while no significant differences were observed in axial stiffness (Fig. 3(*k*)) across genotypes or sex. Finally, so-called distensibility was significantly lower only in the female LPA KOs compared to WTs (LPA: FWT: 340.55 ± 19.98 MPa^{-1}, FKO: 222.84 ± 15.06 MPa^{-1}; Fig. 3(*l*)). These trends were similar at 15 mmHg, although with altered significance in differences (not shown). Sex differences were observed in the loaded diameter, circumferential stretch, and distensibility of the LPA, and the loaded diameter, circumferential stiffness, and axial stretch of the RPA.

H&E stains suggest a thickened right ventricular (RV) free wall in KOs (FWT: 0.42 ± 0.01 mm, FKO: 0.48 ± 0.01 mm, MWT: 0.47 ± 0.01 mm, MKO: 0.57 ± 0.02 mm; Figs. 4(*a*), 4(*b*)). RV thickness was significantly lower in the female WTs compared to male WTs. RV lumen area was significantly different between WTs (FWT:2.82 ± 0.11 mm^2, MWT: 3.63 ± 0.08 mm^2, Fig. 4(*c*)), but not between KOs or genotypes. Cardiac measurements from transthoracic echocardiograms are summarized in Fig. 4. The male KO group had a significantly lower heart rate (HR) than the male WT. HR was also significantly different between sexes—the female WT group had a lower HR than the male WT group, but the female KO had a higher HR than the male KO group (FWT: 421 ± 8.39 beats per minute (bpm), FKO: 415 ± 8.56 bpm, MWT: 467.3 ± 7.02 bpm, MKO: 370.7 ± 7.90 bpm; Fig. 4(*d*)). The KOs trended toward a higher RV stroke volume (Fig. 4(*e*)) and cardiac output (Fig. 4(*f*)) than the WTs, but the differences were not significant. No significant differences in RVOT diameters (Fig. 4(*g*)) were observed between genotypes or sex. TAPSE (Fig. 4(*h*)) was lower in the KO groups but not significantly. FAC was lower in KO, again only significantly so in males (MWT: 42.13 ± 1.77, MKO: 20.73 ± 1.98; Fig. 4(*i*)). In contrast, RA area was higher in the KO groups compared to corresponding WTs but the difference was significant only in the female groups (FWT: 4.37 ± 0.21, FKO: 5.88 ± 0.31; Fig. 4(*j*)). PAT:PET ratio was lower in KO compared to corresponding WTs but differences were not significant (Fig. 4(*k*)).

Discussion

Mouse models can be invaluable in exploring effects of individual proteins on tissue and organ function. While considerable attention has focused on the systemic circulation of elastopathic mice [19,34–39], data remain limited for the pulmonary system, especially in the quantification of lung function and associated pulmonary artery mechanics, with few notable exceptions [14,15]. Remodeling of collagen and associated effects on arterial mechanics have been reported for diverse vessels, including pulmonary

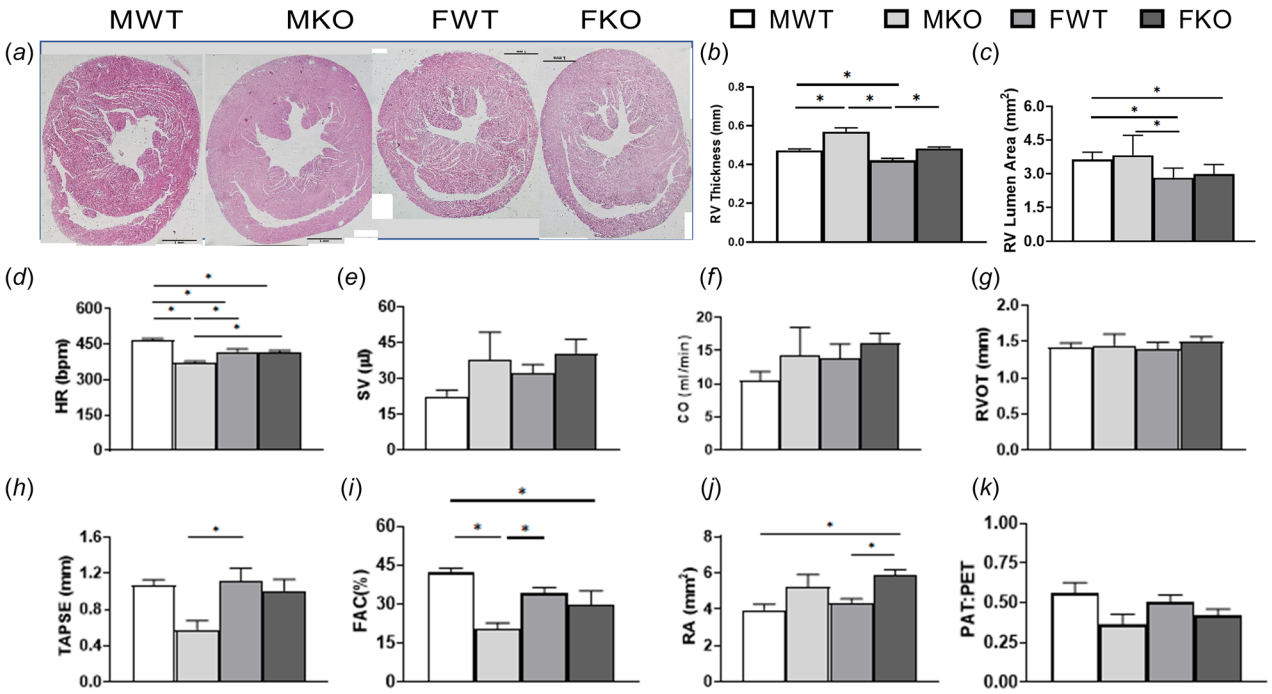

Fig. 4 Representative hematoxylin and eosin (H&E) stained short-axis heart sections of *Fbln5*$^{+/+}$ (WT) and *Fbln5*$^{-/-}$ (KO) mice shown at 4X (*a*). Right ventricle (RV) lumen area (*b*) and wall thickness (*c*) measurements from H&E sections (n = 4). Heart rate (HR; *d*), stroke volume (SV; *e*), cardiac output (CO; *f*), right ventricle outflow tract measurement (RVOT; *g*), tricuspid annular plane systolic excursion (TAPSE; *h*), fractional area change (FAC, *i*), right atrial area (RA; *j*), and ratio of pulmonary acceleration time to ejection time (PAT:PET, *k*) from transthoracic echocardiograms of *Fbln5*$^{+/+}$(WT) and *Fbln5*$^{-/-}$ (KO) mice; female (F), male (M); FWT: n = 5, FKO: n = 4, MWT: n = 4, MKO: n = 3. *$p < 0.05$.

arteries [40], but similar quantifications on elastopathic mouse models are few [14,15]. At the same time, emphysematous changes have been reported in fibulin-5 deficient mice [11,12], though without quantification of lung function or associated vascular and right heart function. Here, we quantified lung parenchymal and pulmonary vascular structure, lung function, pulmonary arterial mechanical properties, and right heart function in adult mice of both sexes in the presence and absence of compromised elastic fiber integrity.

Lung structure and function have been evaluated in a human bacterial artificial chromosome (hBAC) modified mouse model deficient in murine elastin (hBAC-mNULL). Similar to findings in these mice [15], the fibulin-5 KO mice studied herein showed a greater chord length and increased static compliance when compared to WT. Prior findings have shown that fibulin-5 is differentially upregulated in pulmonary arteries in response to hypoxia in mice that overexpress the calcium-binding protein S100A4/Mts1 [41]. Mutations in *FBLN5* have also been linked to severe lung disease in humans with cutis laxa [3,42]. Fibulin-5 protein levels were altered in COPD human lung tissue [13,43]. The fibulin-5 null mice used herein clearly exhibited deficient elastic fiber assembly in the lung as well as emphysematous changes consistent with prior reports [11,12]. This germline mutation thus affects both development and (mal)adaptations subsequent to the defect, thus rendering it a representative model of a congenital or developmental elastic fiber anomaly. Some of the differences we have reported could be due to compensatory adaptations during development, not just the absence of fibulin-5 in the extracellular matrix; this ambiguity is a drawback inherent to any mouse model based on a germline mutation. The present findings may help, nonetheless, in the study of compromised elastogenesis in altering lung function and serve as an accelerated model of aging and cor pulmonale. This model is distinct, however, from primary pulmonary arterial hypertension or Marfan syndrome [2].

Pulmonary arteries from fibulin-5 KO mice exhibit a lower in vivo value of axial stretch, consistent with the lower level of functional elastic fibers and higher collagen content from histology [44]. These histological differences appear to have contributed to the lower wall stresses and elastic energy storage capacity in our KO arteries. Histology confirmed fragmented elastic laminae, which can lead to earlier physical recruitment of collagen fibers at lower stretch [45]. Histological quantification also showed significantly lower elastin content due to both genotype and sex, with lower cytoplasm between genotypes in males but not females. Normal elastin prevents smooth muscle cell proliferation while fragmented elastin may promote it [46]. Sex differences have been documented across multiple pulmonary pathologies involving ventilation-perfusion mismatch, including emphysema and pulmonary hypertension in humans [25,26] and animal models [9,47]. Herein, the cytoplasm content was significantly different between genotypes only in male, not female, pulmonary arteries suggestive of sex differences in developmental adaptations to the knockout. There were also sex differences in static lung compliance in KOs but not WTs. Further imaging would be required to probe effects of damaged elastin on cell morphology as well as collagen structure and load-induced recruitment, especially through development [24,48].

At a microstructural level, the innermost layer of elastin is relatively well preserved in the pulmonary arteries of the fibulin-5 KO mice, while the outer layers exhibit a fragmented structure similar to that reported previously for the thoracic aorta [19]. Whereas differences in wall constituent area fractions were not significant in the thoracic aorta [19], they differed markedly in the pulmonary arteries (Fig. 3). Similarly, sex differences were less pronounced in the thoracic aorta than found herein for the pulmonary arteries (Figs. 2 and 3). Systemic blood pressure is similar between WT and fibulin-5 KO mice at rest [19], yet the descending thoracic aorta exhibits a reduced distensibility and extensibility, a reduced in vivo axial stretch, and an increased wall thickness in the absence of fibulin-5, suggesting that the effects of elastin on arterial remodeling are not solely due to elevated intraluminal pressure. Sex differences in the systemic arteries were few, however,

mainly for the unloaded and loaded diameter which could relate to different body sizes [19].

The right ventricle is known to be enlarged in fibulin-5 KO mice [11], suggestive of elevated right ventricular and pulmonary arterial pressures. We confirmed significant differences in RV mechanics between genotypes (Fig. 4). The RVOT diameter was relatively similar across groups on echocardiographic measurements, suggesting no signs of obstruction or stenosis. TAPSE, a measure of RV systolic function, was significantly reduced in the male KOs suggestive of reduced RV systolic function. Consistent with this, the two-dimensional FAC, another measure of systolic function, trended lower in the KO but was significant only in male KOs. Increased RA size in female KO suggest chronic elevated filling pressures of the RV at end diastole. CO and SV trended higher in the KO groups while PAT:PET ratio was lower in the KO group—a lower PAT:PET ratio correlates well with elevated RV systolic pressure [30,49]. These findings are consistent with changes in the RA and RV after exposure to elevated pressures in the pulmonary circulation. In summary, ultrasound measurements confirm both sex differences and a compromised right heart function in the fibulin-5 deficient mice.

Branch pulmonary arteries play an important role in pulsatility of the blood flow to the distal vasculature and in aiding right heart function. Pulmonary arterial stiffening is associated with adverse outcomes in lung diseases associated with dyspnea, such as COPD and pulmonary hypertension [50–53]. Stiffness is one of the more highly mechano-regulated quantities in systemic vascular adaptations [32,54–56]. Here we quantify it for the pulmonary arteries. Notably, although circumferential stiffness trended lower across genotypes, it was significantly different only in female RPAs. Axial stiffness was similar across regions, sex, and genotype. Increased compliance associated with altered lung parenchyma leads to increased air volumes, or "air-trapping" within the parenchyma, resulting in increased resistance to pulmonary blood flow into the lungs. This is reported to be associated with pulmonary arterial stiffening and decreased distensibility in addition to increased pulmonary vascular resistance [57–61]. Notwithstanding the lack of significance in some groups, our data show that the fibulin-5 deficient pulmonary arteries had a lower loaded outer diameter and distensibility while the lung parenchyma had a higher chord length and compliance (Fig. S3 available in the Supplemental Materials on the ASME Digital Collection). Given that airway disruption has been reported as early as P3 in fibulin-5 KO mice [11], pulmonary artery stiffening may have been a consequence of emphysema. While ventricular-vascular coupling has been studied before [62,63], our data suggest the need for further studies of ventricular-vascular-perfusion coupling. The opposite effects of elastin dysfunction on the parenchyma (increased compliance) and arteries (decreased distensibility; albeit not significant in our study), the interplay between them, and their role in hastening organ-level pathological processes needs to be probed further (Fig. S2 available in the Supplemental Materials on the ASME Digital Collection).

Lack of measurements on the pulmonary pressures and vasoactive tone are limitations of this study. Our current efforts are directed toward invasive and noninvasive measurements. We have also recently developed an in vitro methodology to quantify vasoactive responses of pulmonary arteries in a physiologically realistic biaxial setting [17]. Applying it to fibulin-5 KO mice might shed more light on vasoactive changes in the vasculature and would be a logical next step for this work. Probing adaptations at cellular and molecular scales will be key to understanding sex differences in this mouse model [64–66]. Logistical and workflow constraints prevented vascular, pulmonary, and cardiac measurements on the same mouse herein. Hence, the results presented here are most-representative, though a drawback inherent to most multimodal data collection pipelines. Finally, many of the measurements showed clear trends between genotypes, but statistical significance was not reached (e.g., cardiac measurements). Biologic and measurement variability and small sample sizes may have been the reason for lack of significance, but the results are suggestive nonetheless.

This work shows that a single germline insult (dysfunctional elastic fibers) leads to increased lung parenchymal volume and compliance, stiffened pulmonary arteries with decreased stored energy, and a thickened, compromised right ventricle. Parenchymal changes and the associated changes in pulmonary vascular resistance could be driving the right ventricular remodeling. The lack of definitive methods to uncouple ventilatory, vascular, and right ventricular function remains as a barrier to teasing out coupled contributions of each to the final remodeled states. We nevertheless expect that the present findings will result in better computational models, including image-based pulmonary hemodynamics simulations [67,68], and will also inform models of ventilation and perfusion [69–71]. Such computational models could help elucidate the feedforward and feedback loops involved in pulmonary pathologies. Mouse models help to better isolate causal factors than clinically available human data and are expected to continue to be a promising avenue for building higher fidelity computational models and subsequent hypothesis testing. The data from this study should aid those efforts.

Acknowledgment

We thank Drs. Sae-Il Murtada, Bart Spronck, and Dar Weiss for technical guidance. Dr. Edward Manning is a Pepper Scholar with support from the Claude D. Pepper Older Americans Independence Center at Yale School of Medicine (No. P30AG021342).

Funding Data

- National Institutes of Health (NIH R01 HL105297) (Funder ID: 10.13039/100000002).
- Yale School of Medicine (No. P30AG021342; Funder ID: 10.13039/100007184).

References

[1] Kelly, V. J., Hibbert, K. A., Kohli, P., Kone, M., Greenblatt, E. E., Venegas, J. G., Winkler, T., and Harris, R. S., 2017, "Hypoxic Pulmonary Vasoconstriction Does Not Explain All Regional Perfusion Redistribution in Asthma," Am. J. Respir. Crit. Care Med., **196**(7), pp. 834–844.
[2] Mecham, R. P., 2018, "Elastin in Lung Development and Disease Pathogenesis," Matrix Biol., **73**, pp. 6–20.
[3] Urban, Z., Gao, J., Pope, F. M., and Davis, E. C., 2005, "Autosomal Dominant Cutis Laxa With Severe Lung Disease: Synthesis and Matrix Deposition of Mutant Tropoelastin," J. Invest. Dermatol., **124**(6), pp. 1193–1199.
[4] Taylor, S., Dirir, O., Zamanian, R. T., Rabinovitch, M., and Thompson, A., 2018, "The Role of Neutrophils and Neutrophil Elastase in Pulmonary Arterial Hypertension," Front. Med., **5**, p. 217.
[5] Humbert, M., Guignabert, C., Bonnet, S., Dorfmüller, P., Klinger, J. R., Nicolls, M. R., Olschewski, A. J., Pullamsetti, S. S., Schermuly, R. T., Stenmark, K. R., and Rabinovitch, M., 2019, "Pathology and Pathobiology of Pulmonary Hypertension: State of the Art and Research Perspectives," Eur. Respir. J., **53**(1), p. 1801887.
[6] Humbert, M., Morrell, N. W., Archer, S. L., Stenmark, K. R., MacLean, M. R., Lang, I. M., Christman, B. W., Weir, E. K., Eickelberg, O., Voelkel, N. F., and Rabinovitch, M., 2004, "Cellular and Molecular Pathobiology of Pulmonary Arterial Hypertension," J. Am. Coll. Cardiol., **43**(12), pp. S13–S24.
[7] Stenmark, K. R., and McMurtry, I. F., 2005, "Vascular Remodeling Versus Vasoconstriction in Chronic Hypoxic Pulmonary Hypertension: A Time for Reappraisal?," Am. Heart Assoc., **97**(2), pp. 95–98.
[8] Tojais, N. F., Cao, A., Lai, Y.-J., Wang, L., Chen, P.-I., Alcazar, M. A. A., de Jesus Perez, V. A., Hopper, R. K., Rhodes, C. J., Bill, M. A., Sakai, L. Y., and Rabinovitch, M., 2017, "Codependence of Bone Morphogenetic Protein Receptor 2 and Transforming Growth Factor-β in Elastic Fiber Assembly and Its Perturbation in Pulmonary Arterial Hypertension," Arterioscler. Thromb. Vasc. Biol., **37**(8), pp. 1559–1569.
[9] Stenmark, K. R., Meyrick, B., Galie, N., Mooi, W. J., and McMurtry, I. F., 2009, "Animal Models of Pulmonary Arterial Hypertension: The Hope for Etiological Discovery and Pharmacological Cure," Am. J. Physiol.-Lung Cellular Mol. Physiol., **297**(6), pp. L1013–L1032.
[10] Yanagisawa, H., and Wagenseil, J., 2020, "Elastic Fibers and Biomechanics of the Aorta: Insights From Mouse Studies," Matrix Biol., **85–86**, pp. 160–172.

[11] Nakamura, T., Lozano, P. R., Ikeda, Y., Iwanaga, Y., Hinek, A., Minamisawa, S., Cheng, C.-F., Kobuke, K., Dalton, N., Takada, Y., Tashiro, K., Ross Jr, J., Honjo, T., and Chien, K. R., 2002, "Fibulin-5/DANCE is Essential for Elastogenesis In Vivo," Nature, **415**(6868), pp. 171–175.
[12] Yanagisawa, H., Davis, E. C., Starcher, B. C., Ouchi, T., Yanagisawa, M., Richardson, J. A., and Olson, E. N., 2002, "Fibulin-5 is an Elastin-Binding Protein Essential for Elastic Fibre Development In Vivo," Nature, **415**(6868), pp. 168–171.
[13] Brandsma, C.-A., van den Berge, M., Postma, D. S., Jonker, M. R., Brouwer, S., Paré, P. D., Sin, D. D., Bossé, Y., Laviolette, M., Karjalainen, J., Fehrmann, R. S. N., Nickle, D. C., Hao, K., Spanjer, A. I. R., Timens, W., and Franke, L., 2015, "A Large Lung Gene Expression Study Identifying Fibulin-5 as a Novel Player in Tissue Repair in COPD," Thorax, **70**(1), pp. 21–32.
[14] Shifren, A., Durmowicz, A. G., Knutsen, R. H., Faury, G., and Mecham, R. P., 2008, "Elastin Insufficiency Predisposes to Elevated Pulmonary Circulatory Pressures Through Changes in Elastic Artery Structure," J. Appl. Physiol., **105**(5), pp. 1610–1619.
[15] Shifren, A., Durmowicz, A. G., Knutsen, R. H., Hirano, E., and Mecham, R. P., 2007, "Elastin Protein Levels Are a Vital Modifier Affecting Normal Lung Development and Susceptibility to Emphysema," Am. J. Physiol.-Lung Cellular Mol. Physiol., **292**(3), pp. L778–L787.
[16] Remy-Jardin, M., and Remy, J., 2008, "Vascular Disease in Chronic Obstructive Pulmonary Disease," Proc. Am. Thorac. Soc., **5**(9), pp. 891–899.
[17] Ramachandra, A. B., and Humphrey, J. D., 2019, "Biomechanical Characterization of Murine Pulmonary Arteries," J. Biomech., **84**, pp. 18–26.
[18] Ferruzzi, J., Bersi, M., and Humphrey, J., 2013, "Biomechanical Phenotyping of Central Arteries in Health and Disease: Advantages of and Methods for Murine Models," Ann. Biomed. Eng., **41**(7), pp. 1311–1330.
[19] Ferruzzi, J., Bersi, M., Uman, S., Yanagisawa, H., and Humphrey, J., 2015, "Decreased Elastic Energy Storage, Not Increased Material Stiffness, Characterizes Central Artery Dysfunction in Fibulin-5 Deficiency Independent of Sex," ASME J. Biomech. Eng., **137**(3), p. 031007.
[20] Bersi, M. R., Bellini, C., Wu, J., Montaniel, K. R., Harrison, D. G., and Humphrey, J. D., 2016, "Excessive Adventitial Remodeling Leads to Early Aortic Maladaptation in Angiotensin-Induced Hypertension," Hypertens., **67**(5), pp. 890–896.
[21] Ferruzzi, J., Madziva, D., Caulk, A., Tellides, G., and Humphrey, J., 2018, "Compromised Mechanical Homeostasis in Arterial Aging and Associated Cardiovascular Consequences," Biomech. Model. Mechanobiol., **17**(5), pp. 1281–1295.
[22] Ferruzzi, J., Di Achille, P., Tellides, G., and Humphrey, J. D., 2018, "Combining In Vivo and In Vitro Biomechanical Data Reveals Key Roles of Perivascular Tethering in Central Artery Function," PloS One, **13**(9), p. e0201379.
[23] Murtada, S.-I., Kawamura, Y., Caulk, A. W., Ahmadzadeh, H., Mikush, N., Zimmerman, K., Kavanagh, D., Weiss, D., Latorre, M., Zhuang, Z. W., Shadel, G. S., Braddock, D. T., and Humphrey, J. D., 2020, "Paradoxical Aortic Stiffening and Subsequent Cardiac Dysfunction in Hutchinson–Gilford Progeria Syndrome," J. R. Soc. Interface, **17**(166), p. 20200066.
[24] Pursell, E. R., Vélez-Rendón, D., and Valdez-Jasso, D., 2016, "Biaxial Properties of the Left and Right Pulmonary Arteries in a Monocrotaline Rat Animal Model of Pulmonary Arterial Hypertension," ASME J. Biomech. Eng., **138**(11), p. 111004.
[25] Martinez, F. J., Curtis, J. L., Sciurba, F., Mumford, J., Giardino, N. D., Weinmann, G., Kazerooni, E., Murray, S., 2007, "Sex Differences in Severe Pulmonary Emphysema," Am. J. Respir. Critical Care Med., **176**(3), pp. 243–252.
[26] Hester, J., Ventetuolo, C., and Lahm, T., 2011, "Sex, Gender, and Sex Hormones in Pulmonary Hypertension and Right Ventricular Failure," Comprehensive Physiol., **10**(1), pp. 125–170.
[27] Nouws, J., Wan, F., Finnemore, E., Roque, W., Kim, S.-J., Bazan, I., Li, C.-X., 2021, "MicroRNA miR-24-3p Reduces DNA Damage Responses, Apoptosis, and Susceptibility to Chronic Obstructive Pulmonary Disease," JCI Insight, **6**(2), p. e134218.
[28] Kim, S. -J., Shan, P., Hwangbo, C., Zhang, Y., Min, J. -N., Zhang, X., Ardito, T., Li, A., Peng, T., Sauler, M., and Lee, P. J., 2019, "Endothelial Toll-Like Receptor 4 Maintains Lung Integrity Via Epigenetic Suppression of p16INK4a," Aging Cell, **18**(3), p. e12914.
[29] Lindsey, M. L., Kassiri, Z., Virag, J. A., de Castro Brás, L. E., and Scherrer-Crosbie, M., 2018, "Guidelines for Measuring Cardiac Physiology in Mice," Am. J. Physiol.-Heart Circ. Physiol., **314**(4), pp. H733–H752.
[30] Kohut, A., Patel, N., and Singh, H., 2016, "Comprehensive Echocardiographic Assessment of the Right Ventricle in Murine Models," J. Cardiovas. Ultrasound, **24**(3), pp. 229–238.
[31] Humphrey, J. D., 2013, *Cardiovascular Solid Mechanics: Cells, Tissues, and Organs*, Springer Science & Business Media, Berlin.
[32] Bersi, M., Khosravi, R., Wujciak, A., Harrison, D., and Humphrey, J., 2017, "Differential Cell-Matrix Mechanoadaptations and Inflammation Drive Regional Propensities to Aortic Fibrosis, Aneurysm or Dissection in Hypertension," J. R. Soc. Interface, **14**(136), p. 20170327.
[33] Crowley, G., Kwon, S., Caraher, E. J., Haider, S. H., Lam, R., Batra, P., Melles, D., Liu, M., and Nolan, A., 2019, "Quantitative Lung Morphology: Semi-Automated Measurement of Mean Linear Intercept," BMC Pulm. Med., **19**(1), p. 206.
[34] Le, V. P., Cheng, J. K., Kim, J., Staiculescu, M. C., Ficker, S. W., Sheth, S. C., Bhayani, S. A., Mecham, R. P., Yanagisawa, H., and Wagenseil, J. E., 2015, "Mechanical Factors Direct Mouse Aortic Remodelling During Early Maturation," J. R. Soc. Interface, **12**(104), p. 20141350.
[35] Le, V. P., Stoka, K. V., Yanagisawa, H., and Wagenseil, J. E., 2014, "Fibulin-5 Null Mice With Decreased Arterial Compliance Maintain Normal Systolic Left Ventricular Function, but Not Diastolic Function During Maturation," Physiol. Reports, **2**(3), p. e00257.
[36] Murtada, S.-I., Ferruzzi, J., Yanagisawa, H., and Humphrey, J., 2016, "Reduced Biaxial Contractility in the Descending Thoracic Aorta of Fibulin-5 Deficient Mice," ASME J. Biomech. Eng., **138**(5), p. 051008.
[37] Jiao, Y., Li, G., Korneva, A., Caulk, A. W., Qin, L., Bersi, M. R., Li, Q., Li, W., Mecham, R. P., Humphrey, J. D., and Tellides, G., 2017, "Deficient Circumferential Growth is the Primary Determinant of Aortic Obstruction Attributable to Partial Elastin Deficiency," Aeterioscler, Thrombo., Vasc. Biol., **37**(5), pp. 930–941.
[38] Kozel, B. A., Knutsen, R. H., Ye, L., Ciliberto, C. H., Broekelmann, T. J., and Mecham, R. P., 2011, "Genetic Modifiers of Cardiovascular Phenotype Caused by Elastin Haploinsufficiency Act by Extrinsic Noncomplementation," J. Biol. Chem., **286**(52), pp. 44926–44936.
[39] Faury, G., Pezet, M., Knutsen, R. H., Boyle, W. A., Heximer, S. P., McLean, S. E., Minkes, R. K., Blumer, K. J., Kovacs, A., Kelly, D. P., Li, D. Y., Starcher, B., and Mecham, R. P., 2003, "Developmental Adaptation of the Mouse Cardiovascular System to Elastin Haploinsufficiency," J. Clin. Investig., **112**(9), pp. 1419–1428.
[40] Wang, Z., and Chesler, N. C., 2012, "Role of Collagen Content and Cross-Linking in Large Pulmonary Arterial Stiffening After Chronic Hypoxia," Biomech. Model. Mechanobiol., **11**(1–2), pp. 279–289.
[41] Merklinger, S. L., Wagner, R. A., Spiekerkoetter, E., Hinek, A., Knutsen, R. H., Kabir, M. G., Desai, K., Hacker, S., Wang, L., Cann, G. M., Ambartsumian, N. S., Lukanidin, E., Bernstein, D., Husain, M., Mecham, R. P., Starcher, B., Yanagisawa, H., and Rabinovitch, M., 2005, "Increased Fibulin-5 and Elastin in S100A4/Mts1 Mice With Pulmonary Hypertension," Circulation Res., **97**(6), pp. 596–604.
[42] Mutlu-Albayrak, H., Emiralioğlu, N., and Damar, Ç., 2020, "Overview of the Pulmonary Manifestations in Patients With Autosomal Recessive Cutis Laxa Type IC," Pediatric Allergy, Immunol., Pulmonol., **33**(4), pp. 207–212.
[43] García-Valero, J., Olloquequi, J., Rodríguez, E., Martín-Satué, M., Texidó, L., and Ferrer, J., 2021, "Decreased Expression of EC-SOD and Fibulin-5 in Alveolar Walls of Lungs From COPD Patients," Archivos de Bronconeumología.
[44] Humphrey, J., Eberth, J., Dye, W., and Gleason, R., 2009, "Fundamental Role of Axial Stress in Compensatory Adaptations by Arteries," J. Biomech., **42**(1), pp. 1–8.
[45] Ferruzzi, J., Collins, M. J., Yeh, A. T., and Humphrey, J. D., 2011, "Mechanical Assessment of Elastin Integrity in Fibrillin-1-Deficient Carotid Arteries: Implications for Marfan Syndrome," Cardiovasc. Res., **92**(2), pp. 287–295.
[46] Urbán, Z., Riazi, S., Seidl, T. L., Katahira, J., Smoot, L. B., Chitayat, D., Boyd, C. D., and Hinek, A., 2002, "Connection Between Elastin Haploinsufficiency and Increased Cell Proliferation in Patients With Supravalvular Aortic Stenosis and Williams-Beuren Syndrome," Am. J. Human Genet., **71**(1), pp. 30–44.
[47] Gomez-Arroyo, J., Saleem, S. J., Mizuno, S., Syed, A. A., Bogaard, H. J., Abbate, A., Taraseviciene-Stewart, L., Sung, Y., Kraskauskas, D., Farkas, D., Conrad, D. H., Nicolls, M. R., and Voelkel, N. F., 2012, "A Brief Overview of Mouse Models of Pulmonary Arterial Hypertension: Problems and Prospects," Am. J. Physiol.-Lung Cellular Mol. Physiol., **302**(10), pp. L977–L991.
[48] Cavinato, C., Murtada, S.-I., Rojas, A., and Humphrey, J. D., 2021, "Evolving Structure-Function Relations During Aortic Maturation and Aging Revealed by Multiphoton Microscopy," Mech. Ageing Develop., **196**, p. 111471.
[49] Thibault, H. L. N. B., Kurtz, B., Raher, M. J., Shaik, R. S., Waxman, A., Derumeaux, G. V., Halpern, E. F., Bloch, K. D., and Scherrer-Crosbie, M., 2010, "Noninvasive Assessment of Murine Pulmonary Arterial Pressure: Validation and Application to Models of Pulmonary Hypertension," Circ. Cardiovasc. Imaging, **3**(2), pp. 157–163.
[50] Sanz, J., Prat-Gonzalez, S., Macaluso, F., Fuster, V., and Garcia, M., 2008, "155 Quantification of Pulse Wave Velocity in the Pulmonary Artery in Patients With Pulmonary Hypertension," J. Cardiovasc. Magn. Resonance, **10**(S1), p. A56.
[51] Vivodtzev, I., Minet, C., Tamisier, R., Arbib, F., Borel, J.-C., Baguet, J.-P., Lévy, P., and Pépin, J.-L., 2013, "Arterial Stiffness by Pulse Wave Velocity in COPD: Reliability and Reproducibility," Eur. Respir. J., **42**(4), pp. 1140–1142.
[52] Weir-McCall, J. R., Liu-Shiu-Cheong, P. S., Struthers, A. D., Lipworth, B. J., and Houston, J. G., 2018, "Pulmonary Arterial Stiffening in COPD and Its Implications for Right Ventricular Remodelling," Eur. Radiol., **28**(8), pp. 3464–3472.
[53] Prins, K. W., Weir, E. K., Archer, S. L., Markowitz, J., Rose, L., Pritzker, M., Madlon-Kay, R., and Thenappan, T., 2016, "Pulmonary Pulse Wave Transit Time is Associated With Right Ventricular-Pulmonary Artery Coupling in Pulmonary Arterial Hypertension," Pulm. Circ., **6**(4), pp. 576–585.
[54] Shadwick, R. E., 1999, "Mechanical Design in Arteries," J. Exp. Biol., **202**(23), pp. 3305–3313.
[55] Wagenseil, J. E., and Mecham, R. P., 2009, "Vascular Extracellular Matrix and Arterial Mechanics," Physiol. Rev., **89**(3), pp. 957–989.
[56] Bellini, C., Bersi, M., Caulk, A., Ferruzzi, J., Milewicz, D., Ramirez, F., Rifkin, D., Tellides, G., Yanagisawa, H., and Humphrey, J., 2017, "Comparison of 10 Murine Models Reveals a Distinct Biomechanical Phenotype in Thoracic Aortic Aneurysms," J. R. Soc. Interface, **14**(130), p. 20161036.
[57] Harkness, L. M., Kanabar, V., Sharma, H. S., Westergren-Thorsson, G., and Larsson-Callerfelt, A.-K., 2014, "Pulmonary Vascular Changes in Asthma and COPD," Pulm. Pharmacol. Ther., **29**(2), pp. 144–155.

[58] Ertan, C., Tarakci, N., Ozeke, O., and Demir, A. D., 2013, "Pulmonary Artery Distensibility in Chronic Obstructive Pulmonary Disease," Echocardiography, **30**(8), pp. 940–944.
[59] Rahaghi, F. N., van Beek, E. J. R., and Washko, G. R., 2014, "Cardiopulmonary Coupling in Chronic Obstructive Pulmonary Disease: The Role of Imaging," J. Thorac. Imaging, **29**(2), pp. 80–91.
[60] Sakao, S., Voelkel, N. F., and Tatsumi, K., 2014, "The Vascular Bed in COPD: Pulmonary Hypertension and Pulmonary Vascular Alterations," Eur. Respiratory Rev., **23**(133), pp. 350–355.
[61] Voelkel, N. F., and Cool, C. D., 2003, "Pulmonary Vascular Involvement in Chronic Obstructive Pulmonary Disease," Eur. Respir. J., **22**(Suppl 46), pp. 28 s–32 s.
[62] Bellofiore, A., and Chesler, N. C., 2013, "Methods for Measuring Right Ventricular Function and Hemodynamic Coupling With the Pulmonary Vasculature," Ann. Biomed. Eng., **41**(7), pp. 1384–1398.
[63] Fourie, P. R., Coetzee, A. R., and Bolliger, C. T., 1992, "Pulmonary Artery Compliance: Its Role in Right Ventricular-Arterial Coupling," Cardiovasc. Res., **26**(9), pp. 839–844.
[64] Manning, E. P., Ramachandra, A. B., Schupp, J. C., Cavinato, C., Raredon, M. S. B., Bärnthaler, T., Cosme, C., Singh, I., Tellides, G., Kaminski, N., and Humphrey, J. D., 2021, "Mechanisms of Hypoxia-Induced Pulmonary Arterial Stiffening in Mice Revealed by a Functional Genetics Assay of Structural, Functional, and Transcriptomic Data," Front. Physiol., **1**, epub.
[65] Liu, A., Schreier, D., Tian, L., Eickhoff, J. C., Wang, Z., Hacker, T. A., and Chesler, N. C., 2014, "Direct and Indirect Protection of Right Ventricular Function by Estrogen in an Experimental Model of Pulmonary Arterial Hypertension," Am. J. Physiol.-Heart Circ. Physiol., **307**(3), pp. H273–H283.
[66] Frump, A. L., Albrecht, M., Yakubov, B., Breuils-Bonnet, S., Nadeau, V., Tremblay, E., Potus, F., Omura, J., Cook, T., Fisher, A., Rodriguez, B., Brown, R. D., Stenmark, K. R., Rubinstein, C. D., Krentz, K., Tabima, D. M., Li, R., Sun, X., Chesler, N. C., Provencher, S., Bonnet, S., and Lahm, T., 2021, "17β-Estradiol and Estrogen Receptor α Protect Right Ventricular Function in Pulmonary Hypertension Via BMPR2 and Apelin," J. Clinic. Investig., **131**(6), p. e129433.
[67] Cuomo, F., Ferruzzi, J., Agarwal, P., Li, C., Zhuang, Z. W., Humphrey, J. D., and Figueroa, C. A., 2019, "Sex-Dependent Differences in Central Artery Haemodynamics in Normal and Fibulin-5 Deficient Mice: Implications for Ageing," Proc. R. Soc. A, **475**(2221), p. 20180076.
[68] Yang, W., Dong, M., Rabinovitch, M., Chan, F. P., Marsden, A. L., and Feinstein, J. A., 2019, "Evolution of Hemodynamic Forces in the Pulmonary Tree With Progressively Worsening Pulmonary Arterial Hypertension in Pediatric Patients," Biomech. Model. Mechanobiol., **18**(3), pp. 779–796.
[69] Qureshi, M. U., Colebank, M. J., Paun, L. M., Fix, L. E., Chesler, N., Haider, M. A., Hill, N. A., Husmeier, D., and Olufsen, M. S., 2019, "Hemodynamic Assessment of Pulmonary Hypertension in Mice: A Model-Based Analysis of the Disease Mechanism," Biomech. Model. Mechanobiol., **18**(1), pp. 219–243.
[70] Hasler, D., Anagnostopoulou, P., Nyilas, S., Latzin, P., Schittny, J., and Obrist, D., 2019, "A Multi-Scale Model of Gas Transport in the Lung to Study Heterogeneous Lung Ventilation During the Multiple-Breath Washout Test," PLoS Comput. Biol., **15**(6), p. e1007079.
[71] Marquis, A. D., Jezek, F., Pinsky, D. J., and Beard, D. A., 2021, "Hypoxic Pulmonary Vasoconstriction as a Regulator of Alveolar-Capillary Oxygen Flux: A Computational Model of Ventilation-Perfusion Matching," PLOS Comput. Biol., **17**(5), p. e1008861.